Alma Mater Studiorum Università di Bologna
Archivio istituzionale della ricerca

A solution of Jupiter's gravitational field from Juno data with the ORBIT14 software

This is the final peer-reviewed author's accepted manuscript (postprint) of the following publication:

This version is available at: https://hdl.handle.net/11585/707206 since: 2022-10-21

Published:

DOI: http://doi.org/10.1093/mnras/stz2657

Terms of use:

(Article begins on next page)

A Solution of Jupiter's Gravitational Field from *Juno* Data with the ORBIT14 Software

Daniele Serra,[1]* Giacomo Lari,[1] Giacomo Tommei,[1] Daniele Durante,[2]
Luis Gomez Casajus,[3] Virginia Notaro,[2] Marco Zannoni,[3]
Luciano Iess,[2] Paolo Tortora[3] Scott J. Bolton[4]

[1]*University of Pisa, Pisa, Italy*
[2]*University of Rome La Sapienza, Rome, Italy*
[3]*University of Bologna, Forlì, Italy*
[4]*Southwest Reasearch Institute, San Antonio, Texas, USA*

ABSTRACT

The latest estimation of Jupiter's gravitational field was obtained by processing the Doppler data from two gravity orbits of NASA's *Juno* mission, using the Jet Propulsion Laboratory software MONTE. In this work we present the results of the analysis of the same measurements employing the orbit determination software ORBIT14, developed at the University of Pisa, used here for the first time with real data. We found that the estimated values of Jupiter's spherical harmonic coefficients from the two solutions are consistent within the formal uncertainty. The analysis is complemented with a discussion on the results obtained with alternative setups.

Key words: gravitation – planets and satellites: interiors – planets and satellites: gaseous planets – methods: data analysis

1 INTRODUCTION

Juno is a NASA *New Frontiers* mission which is currently exploring the planet Jupiter by means of a spinning orbiter. On July 5th 2016, the *Juno* spacecraft was inserted into a highly-elliptical 53.5-day polar orbit with perijove altitude of about 4000 km relative to an oblate Jupiter of equatorial radius R_J = 71492 km. Science operations are possible thanks to the nine instruments which compose the orbiter's payload (Bolton 2010). By the end of the nominal mission in 2021, *Juno* will have provided a deeper insight into various aspects of Jupiter's interior, magnetosphere and atmosphere (Matousek 2007).

Juno's gravity experiment, enabled by the onboard Ka-band Translator (Ciarcia et al. 2013) is undertaken during a period of 6-8 hours around perijove, indicated by PJ. The main objective of the experiment is the determination of Jupiter's gravity field, which is a key element for discriminating amongst different models of the planet's interior. Thanks to the presence of a multi-frequency radio link, at X band (7.2 GHz uplink/8.4 GHz downlink) and – for the first time on a Jupiter mission – Ka band (34.4 GHz uplink/32.1 GHz downlink), it is possible to collect very accurate measurements of the orbiter's range-rate, the nominal noise being

$\sim$ 3 μm/s at a conventional 1000 s integration time. These data are then processed to reconstruct the spacecraft's orbit and to determine a set of dynamical parameters that influence the motion of the orbiter. Among them, of particular interest are the parameters describing Jupiter's gravity field, i.e., the spherical harmonic coefficients $C_{\ell m}, S_{\ell m}$ (see Section 3). They are associated with the planet's density profile and allow to infer features of the interior structure (Zharkov & Trubitsyn 1974), especially the zonal coefficients $J_\ell = -C_{\ell 0}$, also known as gravitational momenta (Guillot & Gautier 2007). Not only are the zonal coefficients crucial for the investigation of the interiors of a planet, but a good knowledge of their values is also essential for possible future tests of fundamental physics (Iorio 2019).

Previous Jupiter missions include the *Pioneer* and *Voyager* spacecrafts' fly-bys of the planet in the 1970s, and the *Galileo* mission in the 1990s. The first two, endowed with a S-band communication system, provided a first solution of Jupiter's gravity field up to degree ℓ = 6 (Campbell & Synnott 1985). *Galileo* could not improve this estimation because of a failure of the high gain antenna, which should have enabled a more accurate X-band link. The *Juno* mission has changed the perspective. A first solution with *Juno* regarding the even zonal harmonic coefficients up to degree ℓ = 8 was obtained by processing the Doppler data from the first two perijoves, PJ1 and PJ2, improving

* E-mail: daniele.serra@dm.unipi.it

Table 1. Comparison of values of Jupiter zonal coefficients J_2, J_3, J_4 and J_6 from: (CS85) the solution from combined Pioneer and Voyager data (Campbell & Synnott 1985); (F+17) the solution from Juno PJ1 and PJ2 X-band data (Folkner et al. 2017); (I+18) the solution from Juno PJ3 and PJ6 Ka-band data (Iess et al. 2018). Note that in (I+18) it has been found that the J_3 value is statistically different from zero.

Coefficient	CS85	F+17	I+18
$J_2(\times 10^6)$	14736 ± 1	14696.514 ± 0.272	14696.572 ± 0.014
$J_3(\times 10^6)$	1.4 ± 5	-0.067 ± 0.458	-0.042 ± 0.010
$J_4(\times 10^6)$	-587 ± 5	-586.623 ± 0.363	-586.609 ± 0.004
$J_6(\times 10^6)$	31 ± 20	34.244 ± 0.236	34.198 ± 0.009

Table 2. Date, perijove time, perijove pass duration and Sun-Earth-Probe (SEP) angle of the first two *Juno* gravity passes PJ3 and PJ6. Time is UTC Spacecraft Event Time.

	Date	Perijove time	Perijove pass duration	SEP angle (deg)
PJ3	11 DEC 2016	17:03:40	6h 45m	61.6
PJ6	19 MAY 2017	06:00:45	8h 20m	135.4

dent analysis which confirms the most recent results about Jupiter's interior.

the previous knowledge by a factor 5 or more (Folkner et al. 2017), even if only X/X and X/Ka links were available. The latest published estimation (Iess et al. 2018) takes advantage of the Ka/Ka link of perijoves PJ3 and PJ6 to further improve the accuracy on the even zonal harmonic coefficients up to degree 10 by a factor at least 10 (see Table 1 for a comparison of coefficients J_2, J_4 and J_6). Moreover, the same work presented, for the first time, non-zero values for the odd zonal harmonic coefficients, J_3, J_5, J_7 and J_9. The unprecedented accuracy of these results led to determine that the penetration depth of Jupiter's zonal winds is ~ 3000 km (Kaspi et al. 2018), and to conclude that the deep interior of the planet rotates nearly as a rigid body (Guillot et al. 2018).

Both *Juno* analyses described above were carried out using MONTE, the orbit determination program developed by the Jet Propulsion Laboratory (Evans et al. 2018). In this paper we present a solution of Jupiter's gravity field from *Juno* PJ3 and PJ6 data, obtained independently of the others. The analysis hereby described was performed using the ORBIT14 orbit determination software developed at the University of Pisa, Department of Mathematics. The code was specifically designed for the Radio Science data analysis of ESA/JAXA's mission *BepiColombo* and NASA's mission *Juno*. The main fundamental difference with MONTE is in the relativistic formulation of the N-body dynamics, inasmuch as ORBIT14 implements a multi-chart approach instead of the equivalent single-chart one used by MONTE (see Section 3 for more details and a comprehensive description of the models and algorithms implemented in the software). Until now, ORBIT14 was only used for performing numerical simulations of: the in-orbit *BepiColombo* MORE experiment (Mercury Orbiter Radio-Science Experiment) (Cicalò et al. 2016; Schettino & Tommei 2016), the *BepiColombo* superior conjunction experiment (Serra et al. 2018), the in-orbit *Juno* gravity experiment (Serra et al. 2016; Tommei et al. 2015), and the *JUICE* gravity experiment (Lari & Milani 2019). Since this is the first time that ORBIT14 was used for real data analysis, aim of this work is to validate the program by showing that it yields a result which is consistent with previous ones. As term of comparison, we chose the latest Jupiter's gravity field estimation from Iess et al. (2018). By adopting the same experiment setup used therein, we show (Section 4) that we determine a gravity field which is fully compatible with our reference. Not only does this contribute to the software validation, but it also provides an indepen-

2 DATA, PRE-PROCESSING, MEDIA CALIBRATIONS

The gravity field solution presented in this paper was obtained processing data from the first two *Juno* orbits dedicated to the gravity experiment, namely PJ3 and PJ6. Details about the times and geometry of such orbits are summarized in Table 2. Deep Space Network (DSN) ground antenna Deep Space Station (DSS) 25 (Goldstone, California), which supports two-way Ka-band communication, was used in both cases during the perijove pass, whereas DSS-43 (Canberra, Australia) was used for post-perijove tracking, transmitting and receiving at X band. During each PJ both Doppler and range data were acquired, the latter available only in X band, with a measurement noise of tens of centimeters.

The open-loop data (Deep Space Network Project Office 2000; Asmar et al. 2017) acquired at the ground station on Earth were pre-processed using a digital phase-locked loop so as to extract the received frequencies to be given as input to the ORBIT14 software for data analysis. The radio signal interacts with the water vapor molecules in the Earth troposphere and with the charged particles in the interplanetary plasma, the Jupiter magnetosphere, and the Earth ionosphere. This results in an accumulation of systematic errors in the data (Iess et al. 2012), which must be removed with successive calibrations.

The time delay in the radio signal propagation caused by the charged particles was negligible for the Ka-band Doppler data collected by DSS-25 because the interplanetary plasma is a dispersive medium, its effect being proportional to the inverse of the square of the signal frequency (Asmar et al. 2005). The delay caused by the signal passing through the Io plasma torus is of the same nature, thus negligible as well (Phipps et al. 2018; Iess et al. 2018). The plasma contribution is not negligible for X-band data, as in the case of the *Juno* range data and post-perijove Doppler data. However, the plasma effect is highly detrimental when the spacecraft is close to solar conjunction, i.e., when the Sun-Earth-Probe (SEP) angle is small. Since the spacecraft is far from solar conjunction during PJ3 and PJ6 (see SEP angle values in Table 2), such effect did not compromise remarkably the quality of the data. The Io plasma torus is not a source of noise for the post-perijove data because the spacecraft was well outside of Jupiter's centrifugal equator during the tracking.

The water vapor contained in the Earth troposphere causes an additional delay in the radio signal, independent

of the signal frequency. An Advanced Water Vapor Radiometer (AWVR) installed at station DSS-25 provided precise *in situ* measurements of water vapor content along the line of sight. The obtained time delays were then applied to the prediction function (Section 3). Since the DSS-43 station is not endowed with a AWVR, tropospheric calibration of the post-perijove data was performed using atmospheric data collected from GPS. Finally, Doppler data were also calibrated for the change in frequency caused by the spin of the spacecraft (Marini 1971).

3 METHODS

In this section we describe the models, algorithms, and the estimation filter implemented in the ORBIT14 program, which allow to determine Jupiter's gravity field from *Juno* data, along with other parameters of interest.

3.1 Orbit determination

The data analysis was undertaken using a non-linear least-squares method (Gauss 1809; Milani & Gronchi 2010; Bierman 2006). The experimental data O_i at times $t_1,\ldots,t_n$ were modelled using a prediction function $C(t,\mathbf{x})$, which depends on a number of parameters $\mathbf{x}$. Let $\xi_i(\mathbf{x}) = O_i - C(t_i,\mathbf{x})$ be the i-th residual and $\boldsymbol{\xi} = (\xi_i)_{i=1,\ldots,n}$. We can obtain an estimate of the parameters by minimizing the target function

$$Q(\mathbf{x}) = \sum_{i=1}^{n} \frac{\xi_i^2(\mathbf{x})}{\sigma_i^2}, \qquad (1)$$

where σ_i^{-1} is the weight assigned to the i-th data point. The minimum condition implies the normal equations, which allow to solve for $\mathbf{x}$:

$$C(\mathbf{x} - \mathbf{x}_0) = -B^T W \boldsymbol{\xi}. \qquad (2)$$

Here, B and C are respectively the design and the normal matrix,

$$B = \frac{\partial \boldsymbol{\xi}}{\partial \mathbf{x}}, \qquad C = B^T W B, \qquad (3)$$

W is the matrix of the weigths, and $\mathbf{x}_0$ is the first guess value of the parameters. The normal equations are solved iteratively until some convergence condition is satisfied. The covariance matrix at convergence $\Gamma = C^{-1}$ holds statistical information about the estimated parameters, such as formal uncertainties and correlations. If some a priori values $\mathbf{x}_{AP}$ of the solve-for parameters are available, e.g., from other space missions, the normal equations are modified as follows:

$$(C + C_{AP})(\mathbf{x} - \mathbf{x}_0) = -B^T W \boldsymbol{\xi} + C_{AP}(\mathbf{x}_{AP} - \mathbf{x}), \qquad (4)$$

where C_{AP} contains the a priori uncertainties of the a priori parameters. In this case the covariance matrix is $(C+C_{AP})^{-1}$.

The data analysis was performed using a multi-arc strategy, which allows to combine the information from different observed arcs – in this case PJ3 and PJ6 – provided that we solve for a set of initial conditions of the spacecraft for each PJ. Parameters only relative to a specific arc, like the spacecraft initial state, are called local parameters, as opposed to the global parameters, which are common to all arcs. The multi-arc strategy was successfully applied to

the analysis of radio science data of several space missions (Modenini & Tortora 2014; Tortora et al. 2016; Iess et al. 2014; Durante et al. 2019). For more information on the multi-arc strategy, see Milani & Gronchi (2010).

3.2 Prediction function and multi-chart approach

The prediction function for the Doppler observable at reception time t_R is obtained integrating the transmitted frequency f over the time interval centered at transmission time $t_T = t_R - \tau$, where τ is the two-way light-time between the ground station and the focal point of the spacecraft's antenna (Moyer 2003). A change of variables in the integral yields the following equivalent formulation, implemented in ORBIT14:

$$C(\bar{t}, \bar{\mathbf{x}}) = \frac{\alpha}{T} \int_{t_R - \frac{T}{2}}^{t_R + \frac{T}{2}} f(t') \left[1 - \frac{2}{c} \dot{\rho}(t) \right] dt, \quad t' = t'(\mathbf{x}) = t - \tau(\mathbf{x}), \qquad (5)$$

where α is the turn-around ratio (a fractional number relative to the signal band), T is the integration time, c is the speed of light, $\dot{\rho}$ is the spacecraft range-rate. The integral is evaluated using a 7-node Gauss quadrature formula, for high precision. The integral formulation of Doppler observable implemented in ORBIT14 is known to be less affected by numerical noise, as compared to the differential formulation implemented in MONTE (Zannoni & Tortora 2013). The details for the computation of τ in ORBIT14 are discussed in Tommei et al. (2010). We limit ourselves to mention that this calculation must take into account the time-delay caused by the curved space-time, usually referred to as Shapiro effect (Shapiro 1964), with contributions from both the Sun and Jupiter. As regards the latter, we also included the effect of Jupiter's J_2 (Serra et al. 2016).

The orbits of the spacecraft, of the Barycenter of the Jovian System (BJS), and of the Earth, expressed in a common relativistic reference frame, are needed for the light-time computation. The first two are obtained via numerical integration, whereas the latter is taken from the Jet Propulsion Laboratory's ephemerides DE438. Numerical integrations are performed following a multi-chart approach (Damour et al. 1994), i.e., considering different space-time reference frames for different bodies. The orbit of the spacecraft is obtained in a local chart centered at Jupiter barycenter, and the orbit of BJS is computed in a reference frame centered at the Solar System Barycenter (SSB). In order to guarantee consistency with the single-chart approach (Moyer 2003), each reference frame is characterized by a different time coordinate: Jupiter Dynamical Time (TDJ) for the Jovian reference frame and Barycentric Dynamical Time (TDB) for the SSB reference frame. Moreover, positions, velocities and accelerations from different frames must be converted to a common frame in order to be compared or summed together. The transformations from a planetocentric chart to a SSB chart for vectors and time coordinates can be found in Tommei et al. (2010).

The Earth rotation, crucial for determining the position of the ground antenna with respect to the Earth barycenter, is obtained using the IERS Earth orientation parameters (Petit & Luzum 2010).

3.3   Spacecraft and Jovian System Barycenter dynamical models

For the integration of the spacecraft's orbit we consider a reference frame centered at Jupiter's center of mass. The main force acting on the spacecraft is Jupiter's gravity field. In a Jupiter-centered body-fixed reference frame, this is modeled using spherical harmonic functions (Kaula 1966), which allow to expand Jupiter's gravitational potential U in an infinite series

$$U = \frac{GM_J}{r} \left\{ 1 + \sum_{\ell=2}^{\infty} \sum_{m=0}^{\ell} \left(\frac{R_J}{r} \right)^{\ell} \left[C_{\ell m} Y_{\ell m1}(\theta, \lambda) + S_{\ell m} Y_{\ell m0}(\theta, \lambda) \right] \right\},$$
(6)

where GM_J is Jupiter's gravitational parameter, θ, λ are the spacecraft's latitude and longitude, r is its distance from the center, and $Y_{\ell m1}, Y_{\ell m0}$ are the spherical harmonic functions. Determining the planet's gravity field is equivalent to determining its spherical harmonic coefficients $C_{\ell m}$, $S_{\ell m}$. Coefficients C_{10}, C_{11} and S_{11} are zero because they correspond to the coordinates of Jupiter's center of mass in the considered reference frame. Another significant perturbation is caused by Jupiter's tidal deformation, induced by the Galilean Satellites and the Sun. This is modelled as corrections to Jupiter's spherical harmonic coefficients $\Delta C_{\ell m}, \Delta S_{\ell m}$ and depends on Jupiter's Love numbers $k_{\ell m}$ (Eanes et al. 1983). Other forces of gravitational nature are: the third-body perturbations due to the Galilean Satellites, the minor satellites Amalthea and Thebe, the Sun, the planets and Pluto; the indirect oblateness forces, induced by the action of Jupiter's gravity harmonics on the Galilean Satellites, Amalthea and Thebe (Lainey et al. 2004), which appear because we are considering a Jupiter-centered frame. The essential relativistic perturbations arising when using a multi-chart approach are the relativistic gravitational acceleration due to Jupiter – also known as Schwarzschild term – and the geodesic precession (Godard et al. 2012). We also included the Lense-Thirring effect, which is proportional to Jupiter's angular momentum magnitude (Mashhoon et al. 1984). The non-gravitational perturbations included in the model are the solar radiation pressure and the force induced by Jupiter's infrared radiation and thermal emission (Milani et al. 1987). For a table of the magnitudes of the forces previously described, see Tommei et al. (2015).

The BJS is defined as the barycenter of the system composed of Jupiter, Io, Europa, Ganymede, Callisto, Amalthea and Thebe. The ephemerides and masses of these bodies are taken from the satellite ephemerides solution Jup310 (Jacobson 2009). Acting on BJS are the point-mass direct accelerations of the Sun, the planets, Pluto and a list of 343 asteroids. We also included the relativistic post-newtonian terms (Milani et al. 2010), where all the post-newtonian parameters are set to their general relativity values and are not estimated because *Juno* cannot improve their current knowledge (Tommei et al. 2015). For recent overviews of general relativity and the challenges it may face after one century after its publication, see, e.g., Iorio (2015), Debono & Smoot (2016) and references therein.

Finally, the considered precession model of Jupiter's rotation axis is a linear one:

$$\alpha(t) = \alpha_0 + \dot{\alpha}(t - t_0), \quad \delta(t) = \delta_0 + \dot{\delta}(t - t_0),$$
(7)

where α, δ are right ascension and declination of the pole, $\dot{\alpha}, \dot{\delta}$ are their rate, $t_0 =$J2000[1] and $\alpha_0 = \alpha(t_0)$, $\delta_0 = \delta(t_0)$.

4   DATA ANALYSIS AND RESULTS

4.1   Experiment setup

Since we are aiming to validate the ORBIT14 orbit determination software, the main setup adopted for the data analysis, i.e., the data considered, the list of estimated parameters and the planetary ephemerides used, is the same of our reference solution Iess et al. (2018).

The Doppler and range data available from PJ3 and PJ6 have been processed so as to obtain a solution of the jovian gravity field. Considering that the time scale of gravity harmonics of degree $\ell = 25$ is $\simeq 150$ s, in order to have proper sampling of the gravity signal the Doppler measurements were compressed to the integration time $T = 60$ s. Range observables were acquired at a rate of one every $300s$ at the ground station. However, range measurements provide a significant contribution only when investigating phenomena with large time scales, as in the case of planetary ephemerides and relativistic effects (Cicalò et al. 2016). Therefore, in the case of Jupiter's gravity field determination with *Juno*, range-rate data have a major role in the experiment.

The estimation scheme had two stages: at first the two PJs were processed independently to detect and delete any outliers, and obtain a first fit; then, the root mean square (RMS) of each PJ's post-fit residuals was used as uniform weight of the corresponding observational data in a PJ3-PJ6 multi-arc fit.

The estimated global parameters were: Jupiter's zonal spherical harmonic coefficients J_{ℓ}, $\ell = 2, \ldots, 24$, Jupiter's non-zonal quadrupole coefficients $C_{21}, S_{21}, C_{22}, S_{22}$, Jupiter's gravitational parameter GM_J, Jupiter's pole right ascension and declination at J2000 α_0, δ_0, Jupiter's rotation axis precession rate parameters $\dot{\alpha}, \dot{\delta}$, Jupiter's Love number k_{22}, and the BJS initial position and velocity. To minimize the propagation error, the BJS initial state vector was estimated at the central time of the interval between the two PJs' dates, i.e., March 1st, 2017. For each PJ we estimated the following set of local parameters: the spacecraft's initial position and velocity and one constant range bias for each station. The spacecraft's initial state vector was estimated at perijove time. For all the gravity field parameters, except GM_J, we set an a priori uncertainty at least 100 larger than the final estimated formal uncertainty. Since *Juno* is not as sensitive to Jupiter's mass as previous missions were, we constrained GM_J with a priori uncertainty from the *Galileo* mission (Jacobson et al. 1999).

4.2   Results and discussion

The set of solve-for parameters selected for the data analysis was enough to obtain zero-mean randomly distributed residuals at convergence of the orbit determination process (Fig. 1). The RMS of the residuals is a measure of the noise of the observables. For the Ka-band data this was ~ 16 μm/s

---
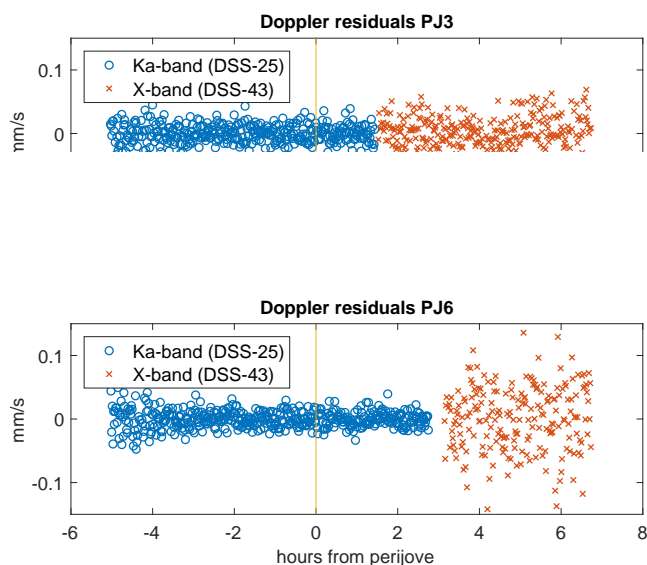
[1] January 1st, 2000, 12:00:00 TDB

Figure 1. Two-way Doppler residuals, expressed in terms of radial velocity, of PJ3 and PJ6, at 60-second integration time. The blue circles refer to the Ka-band data (from DSS-25) and the red crosses to the X-band post-perijove data (from DSS-43). The RMS of the Ka-band is $\sim 16\ \mu$m/s for PJ3 and $\sim 14\ \mu$m/s for PJ6.

Figure 2. Unnormalized Jupiter's zonal spherical harmonic coefficients up to degree 12 from Iess et al. (2018) and from ORBIT14 *Juno* data processing, with 3σ error bars. The first solution is considered as the reference, thus set to zero, whereas the second is represented as difference from the first one. The values of the parameters, their formal uncertainties and their differences in terms of the uncertainty are reported in Table 3.

for PJ3 and $\sim 14\ \mu$m/s for PJ6 at 60 seconds integration time.

Amongst the estimated parameters, we are mostly interested in comparing those regarding Jupiter's gravitational field. In Table 3 we reported the values and three times the formal uncertainties (3σ) of the first 12 zonal harmonic coefficients of Jupiter's gravity field, the non-zonal quadrupole coefficients and the Love number k_{22} from our analysis and from Iess et al. (2018). Zonal coefficients of degree $12 < \ell \leq 24$ do not appear because the signal-to-noise ratio for these parameters turned out being smaller than 1. For immediate visualization, a comparison between the zonal coefficients is represented in Fig. 2. The ORBIT14 estimated gravity parameters resulted to be in very good agreement with the solution from Iess et al. (2018), both in the nominal values and in the formal uncertainty. In particular, as appears from Table 3, the difference between the gravity coefficients from the two solutions is well below the uncertainty reported in Iess et al. (2018). In fact $\sim 80\%$ of all the estimated parameters turned out to be 1σ-compatible, and the remaining ones 2σ-compatible. We remark that the estimated value of k_{22} resulted consistent with the theoretical value predicted by Wahl et al. (2016). As far as the formal uncertainties are concerned, their relative differences are generally below 10%, a few up to 25%. Only for C_{21} sigma, the relative difference is $\sim 40\%$. For all parameters, the uncertainties estimated with ORBIT14 are larger than those estimated with MONTE.

It is worth mentioning that the J2000 pole angles α_0 and δ_0 are highly correlated to the pole rate parameters $\dot{\alpha}$ and $\dot{\delta}$, the correlations being as large as 0.999. This indicates that the effects of such parameters on the Doppler measurements can be hardly separated from each other at this stage. We argue that this is because the time span covered by PJ3 and PJ6 is too small to detect the precession
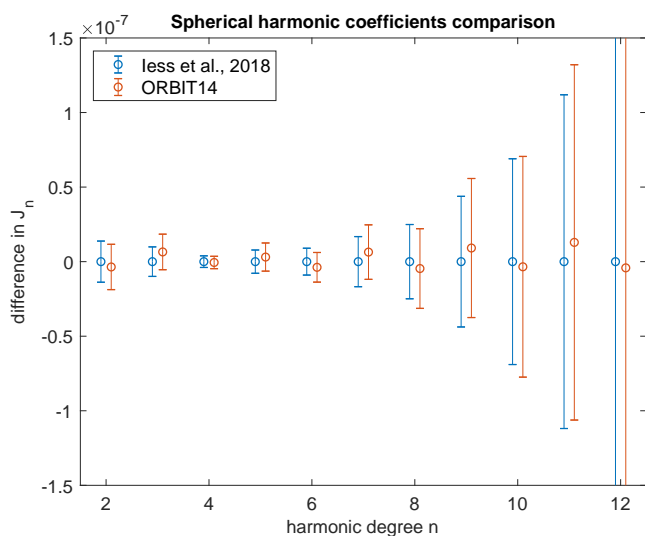
signal. One could question if the pole rate parameters are indeed necessary to our present analysis. From a second experiment carried out with the ORBIT14 software, where we excluded $\dot{\alpha}$ and $\dot{\delta}$ from the setup and fixed them to the value from Jacobson (2009), we indeed obtained values of the gravity field parameters which were compatible with the nominal experiment (Fig. 3). The only difference was in the formal uncertainties of J_2 and the non-zonal quadrupole coefficients, which turned out being smaller by up to a factor of 2. The drop in the uncertainties was expected because the four pole parameters $\alpha_0, \delta_0, \dot{\alpha}, \dot{\delta}$ are also correlated with the degree-2 spherical harmonic coefficients. Thus the pole rate parameters contribute significantly to the gravity field uncertainty. We conclude that, although it is possible to fit the data without the pole rate, it is essential to include it, or the analysis would yield optimistic and illusory accuracies on Jupiter's quadrupole. The precession rate contains critical information about Jupiter's moment of inertia, a key parameter for modeling its interior structure (Iorio 2010; Helled et al. 2011). Although with only PJ3-PJ6 we do not obtain any significant improvement on its knowledge, at the end of the *Juno* mission the situation will dramatically improve. Simulations using the previous two-year long *Juno* mission with a 14-day orbit showed that the precession rate should be determined at the 0.1% level at the end of mission (Le Maistre et al. 2016). Considering that in the actual orbit configuration the total mission duration is about five years, it is possible that the achievable uncertainty will be even smaller.

Finally, it is interesting to remark that including the station DSS-43 data in the analysis leads to a stronger and more accurate solution than the case with only DSS-25 data. At first glance this would appear counterintuitive because the DSS-43 observables are only in X band and far from the pericenter. In fact, the presence of post-perijove observations

Table 3. Unnormalized zonal spherical harmonic coefficients J_ℓ, $\ell = 2, \ldots, 12$, non-zonal quadrupole C_{21}, S_{21}, C_{22}, S_{22}, and k_{22}, estimated with *Juno* data, from Iess et al. (2018) analysis (column 2) and from ORBIT14 analysis (column 3), with 3σ formal uncertainty. The difference between the two solutions is expressed in units of the largest formal uncertainty (column 4, see also Fig. 2). The other two solutions refer to two other ORBIT14 analyses in different setups: not determining the spin pole rate (column 5, see also Fig. 3) and not including DSS-43 data (column 6, see also Fig. 4).

| Parameter	Iess et al., 2018	ORBIT14	Difference (units of σ)	ORBIT14 (pole-rate not estimated)	ORBIT14 (no DSS-43 data)
$J_2(\times 10^6)$	14696.572 ± 0.014	14696.575 ± 0.015	0.7	14696.574 ± 0.006	14696.594 ± 0.049
$J_3(\times 10^6)$	-0.042 ± 0.010	-0.048 ± 0.012	1.6	-0.048 ± 0.011	-0.036 ± 0.022
$J_4(\times 10^6)$	-586.609 ± 0.004	-586.608 ± 0.004	0.4	-586.608 ± 0.004	-586.616 ± 0.012
$J_5(\times 10^6)$	-0.069 ± 0.008	-0.072 ± 0.009	1.0	-0.072 ± 0.008	-0.067 ± 0.016
$J_6(\times 10^6)$	34.198 ± 0.009	34.202 ± 0.010	1.1	34.202 ± 0.009	34.190 ± 0.018
$J_7(\times 10^6)$	0.124 ± 0.017	0.117 ± 0.018	1.0	0.118 ± 0.017	0.130 ± 0.028
$J_8(\times 10^6)$	-2.426 ± 0.025	-2.421 ± 0.027	0.5	-2.421 ± 0.025	-2.445 ± 0.040
$J_9(\times 10^6)$	-0.106 ± 0.044	-0.115 ± 0.046	0.6	-0.115 ± 0.045	-0.087 ± 0.064
$J_{10}(\times 10^6)$	0.172 ± 0.069	0.175 ± 0.074	0.1	0.175 ± 0.071	0.126 ± 0.097
$J_{11}(\times 10^6)$	0.033 ± 0.112	0.020 ± 0.119	0.3	0.020 ± 0.117	0.080 ± 0.150
$J_{12}(\times 10^6)$	0.047 ± 0.178	0.051 ± 0.187	0.1	0.051 ± 0.183	-0.048 ± 0.226
$C_{21}(\times 10^6)$	-0.013 ± 0.015	-0.006 ± 0.025	0.3	-0.007 ± 0.012	0.009 ± 0.044
$S_{21}(\times 10^6)$	-0.003 ± 0.026	-0.017 ± 0.029	0.5	-0.015 ± 0.013	-0.049 ± 0.073
$C_{22}(\times 10^6)$	0.000 ± 0.008	0.002 ± 0.010	0.2	-0.000 ± 0.005	-0.018 ± 0.029
$S_{22}(\times 10^6)$	0.000 ± 0.011	0.008 ± 0.012	0.7	0.007 ± 0.006	0.008 ± 0.022
k_{22}	0.625 ± 0.021	0.589 ± 0.027	1.3	0.589 ± 0.026	0.814 ± 0.285
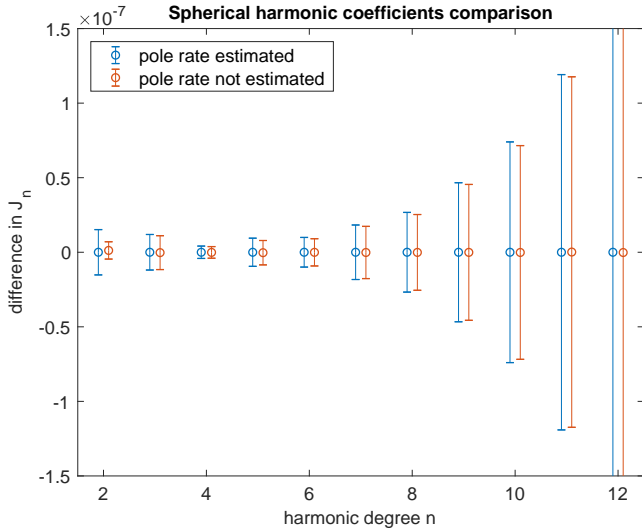
Figure 3. Unnormalized Jupiter's zonal spherical harmonic coefficients up to degree 12 from ORBIT14 *Juno* data processing. The first bar refers to the solution from Table 3, the second bar refers to a solution obtained in the same setup, excluding $\dot\alpha, \dot\delta$ from the list of estimated parameters. The J_2 formal uncertainty in the second solution is underestimated by a factor ~ 2.5. The first solution is here considered as the reference, thus set to zero, whereas the second is represented as difference from the first one.
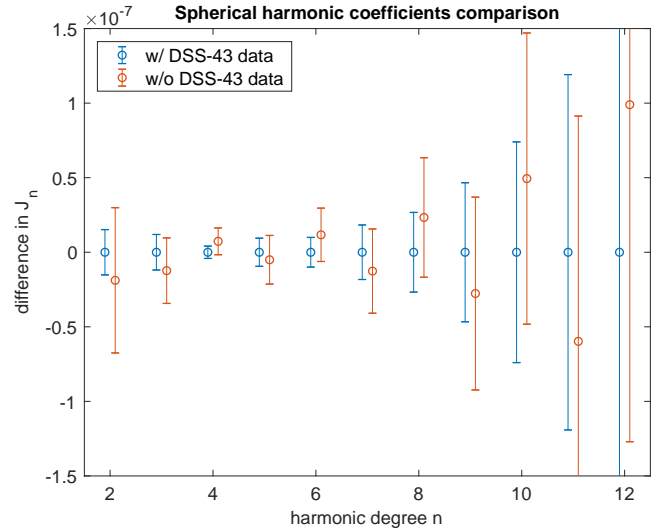
Figure 4. Unnormalized Jupiter's zonal spherical harmonic coefficients up to degree 12 from ORBIT14 *Juno* data processing. The first bar refers to the solution from Table 3, the second bar refers to a solution obtained with the same setup, excluding DSS-43 data from the analysis. Formal uncertainties of the second solution are 2 times larger for $J_3, \ldots, J_{12}$ and 4 times larger for J_2, due to poorer spacecraft orbit determination in the second analysis. The first solution is here considered as the reference, thus set to zero, whereas the second is represented as difference from the first one.

helps to better constrain the state vector of the spacecraft, i.e., its orbit. A better orbit determination helps in turn to separate the effect of different parameters, resulting in a drop in correlations and finally in smaller formal uncertainties for all parameters. In Fig. 4 we compare the ORBIT14 gravitational field solution from Table 3 to the ORBIT14 solution obtained with the same setup, only ignoring the DSS-43 data. The two solutions are still 3σ-coherent, but the formal uncertainties when DSS-43 data are not processed are up to 2 times larger for J_ℓ, $\ell = 3, \ldots, 12$, and ~ 4 times

larger for J_2. Such difference in J_2 uncertainty stems from the fact that the pole angles and the orbit of the spacecraft are highly correlated (~ 0.99), and the pole and J_2 are moderately correlated (~ 0.8): when we fix the orbit using the DSS-43 data we are also able to better separate the pole from J_2, resulting in a considerable gain in terms of formal uncertainty.

5 CONCLUSIONS

In this work we have presented a solution of Jupiter's gravitational field from NASA's *Juno* mission data, obtained using the ORBIT14 orbit determination program developed at the University of Pisa, and compared it to the solution reported in Iess et al. (2018), where the JPL software MONTE was used. The two estimations were undertaken using the same experiment setup, i.e., using the same data and determining the same parameters. However, the two programs implement different mathematical formulations, thus the two analyses are independent of one another.

The Doppler and range data considered were collected during two *Juno* orbits dedicated to gravity science, PJ3 and PJ6. The presence of an on-board Ka-band transponder allowed to acquire high-precision Ka/Ka Doppler data during the perijove passes, thanks to the radio links established with the DSS-25 ground station in Goldstone, California. Doppler and range data were also collected at X band in a post-perijove session from the DSS-43 antenna in Canberra, Australia. The data analysis was undertaken using a least-squares method to estimate a set of parameters which include the zonal spherical harmonic coefficients of Jupiter's gravity field J_ℓ, $\ell = 2, \ldots, 12$, Jupiter's Love number k_{22}, Jupiter's pole right ascension and declination values at time J2000, and Jupiter's pole rate parameters.

We found that the ORBIT14 determination of Jupiter's gravity field was fully consistent with the solution published in Iess et al. (2018), insofar as the difference between the spherical harmonic coefficients estimated in the two analyses was smaller than the formal uncertainties reported therein, and the uncertainties themselves turned out to be comparable.

We went on to point out how Jupiter's pole rate is a critical parameter for our analysis, as it contributes significantly to the degree-2 spherical harmonic coefficients uncertainty, increasing it up to a factor 2.

Finally, we remarked that including the post-perijove X-band data helped to separate the effects of a change in Jupiter's pole angles and J_2 on the spacecraft orbit, therefore allowing a better determination of the orbit itself. This resulted in much smaller formal uncertainties for all gravitational parameters (up to a factor ~ 4, as in the case of J_2), with respect to an analysis where the post-perijove data were not included.

Surely *Juno*'s findings about Jupiter's interior structure are not over yet. At the end of *Juno*'s exploration of the giant planet, the spacecraft will have accomplished about 20 gravity orbits and consequently a lot more radio science data will have been acquired. The estimation of Jupiter's rotation axis precession rate and of the higher-degree Love numbers, for instance, will provide new information about Jupiter's moment of inertia and its tidal response, respectively. When undertaking a high-precision experiment like *Juno*'s, it is crucial to conduct independent analyses, and in this sense a dedicated code like ORBIT14 represents a valuable resource.

References

Asmar S., Armstrong J., Iess L., Tortora P., 2005, Radio Science, 40

Asmar S., et al., 2017, Space Science Reviews, 213, 1

Bierman G. J., 2006, Factorization Methods for Discrete Sequential Estimation. Dover Publications

Bolton S. J., 2010, in Proceedings of the International Astronomical Union. Cambridge Journals, pp 92–100

Campbell J., Synnott S., 1985, Astronomical Journal, 90, 364

Ciarcia S., Simone L., Gelfusa D., Colucci P., De Angelis G., Argentieri F., Iess L., Formaro R., 2013, in 6th ESA International Workshop on Tracking Telemetry and Command Systems for Space Applications.

Cicalò S., Schettino G., Di Ruzza S., Alessi E., Tommei G., Milani A., 2016, Mon. Not. R. Astron. Soc., 457, 1507

Damour T., Soffel M., Xu C., 1994, Phys. Rev. D, 49, 618

Debono I., Smoot G., 2016, Universe, 4

Deep Space Network Project Office 2000, DSN Telecommunications Link Design Handbook, DSN No. 810-005, 209, Rev. C, Jet Propulsion Laboratory, Pasadena, CA

Durante D., Hemingway D., Racioppa P., Iess L., Stevenson D., 2019, Icarus, 326, 123

Eanes R., Schutz B., Tapley B., 1983, in Kuo J., ed., Proceedings of the Ninth International Symposium on Earth Tides.

Evans S., et al., 2018, CEAS Space Journal, 10, 79

Folkner W., et al., 2017, Geophysical Research Letters, 44

Gauss C., 1809, Theoria motus corporum coelestium in sectionis conicis solem ambientum. Hamburg: Friedrich Perthes and I.H. Besser

Godard B., Budnik F., Morley T., Lopez Lozano A., 2012, in Proceedings 23th International Symposium Space Flight Dynamics, Pasadena, CA (USA).

Guillot T., Gautier D., 2007, in Spohn T., Schubert J., eds, , Vol. 10, Treatise of Geophysics: "Planets and Moons". Elsevier Publ., pp 439–464

Guillot T., et al., 2018, Nature, 555, 227

Helled R., Anderson J. D., Schubert G., Stevenson D., 2011, Icarus, 216, 440

Iess L., et al., 2012, Proceedings of the International Astronautical Congress, 5, 3425

Iess L., et al., 2014, Science, 344, 78

Iess L., et al., 2018, Nature, 555, 220

Iorio L., 2010, New Astronomy, 15, 554

Iorio L., 2015, Universe, 1, 38

Iorio L., 2019, Mon. Not. R. Astron. Soc., 484, 4811

Jacobson R., 2009, Jup310 satellite ephemeris file, NASA Navigation and Ancillary Information Facility, https://naif.jpl.nasa.gov/pub/naif/generic_kernels/spk/satellites/jup310.cmt.

Jacobson R., Haw R., McElrath T., Antreasian P., 1999, Adv. Astronaut. Sci., 103, 465

Kaspi Y., et al., 2018, Nature, 555, 223

Kaula W., 1966, Theory of Satellite Geodesy: Applications of Satellites to Geodesy. Dover Publications

Lainey V., Duriez L., Vienne A., 2004, Astron. Astrophys., 420, 1171

Lari G., Milani A., 2019, Planetary and Space Science, 176, 104679

Le Maistre S., Folkner W. M., Jacobson R., Serra D., 2016, Planetary and Space Science, 126, 78

Marini J., 1971, IEEE Transactions on Aerospace and Electronics System, AES-7, 316

Mashhoon B., Hehl F. W., Theiss D., 1984, General Relativity and Gravitation, 16

Matousek S., 2007, Acta Astronautica, 61, 932

Milani A., Gronchi G. F., 2010, Theory of Orbit Determination. Cambridge University Press

Milani A., Nobili A., Farinella P., 1987, Non-gravitational perturbations and satellite geodesy. Adam Hilger Ltd., Bristol,UK

Milani A., Tommei G., Vokrouhlicky D., Latorre E., Cicalò S., 2010, in Relativity in Fundamental Astronomy, Proceedings IAU Symposium No. 261.

Modenini D., Tortora P., 2014, Phys. Rev. D, 90, 022004

Moyer T. D., 2003, Formulation for Observed and Computed Values of Deep Space Network Data Types for Navigation. Wiley-Interscience

Petit G., Luzum B. e., 2010, IERS technical note; 36, IERS Conventions (2010). IERS Conventions Centre

Phipps P., et al., 2018, JGR Space Physics, 8, 6207

Schettino G., Tommei G., 2016, Universe, 2

Serra D., Dimare L., Tommei G., Milani A., 2016, Planetary and Space Science, 134, 100

Serra D., Di Pierri V., Schettino G., Tommei G., 2018, Phys. Rev. D, 98

Shapiro I., 1964, Phys. Rev. Letters, 13, 789

Tommei G., Milani A., Vokrouhlicky D., 2010, Celestial mechanics and dynamical astronomy, 107

Tommei G., Dimare L., Serra D., Milani A., 2015, Monthly Notices of Royal Astronomical Society, 446 (2), 3089

Tortora P., Zannoni M., Hemingway D., Nimmo F., Jacobson R., Iess L., Parisi M., 2016, Icarus, 264, 264

Wahl S., Hubbard W., Militzer B., 2016, The Astrophysical Journal, 831, 14

Zannoni M., Tortora P., 2013, Journal of Guidance Control and Dynamics, 36, 1008

Zharkov V., Trubitsyn V. P., 1974, Icarus, 21, 152